Supplementary Information

for

PhaseT∃M: 3D Imaging at 1.6 Å Resolution via Electron Cryo-Tomography with Nonlinear Phase Retrieval

Juhyeok Lee[1,2*], Samuel W. Song[3], Min Gee Cho[2], Georgios Varnavides[3,4], Stephanie M. Ribet[2], Colin Ophus[5,6], Mary C. Scott[2,3*], Michael L. Whittaker[1,7*]

[1]Energy Geosciences Division, Lawrence Berkeley National Laboratory, Berkeley, 94720, CA, USA.
[2]National Center for Electron Microscopy, Molecular Foundry, Lawrence Berkeley National Laboratory, Berkeley, 94720, CA, USA.
[3]Department of Materials Science and Engineering, University of California Berkeley, Berkeley, 94720, CA, USA.
[4]Miller Institute for Basic Research in Science, University of California Berkeley, Berkeley, 94720, CA, USA.
[5]Department of Materials Science and Engineering, Stanford University, Stanford, 94305, CA, USA.
[6]Precourt Institute for Energy, Stanford University, Stanford, 94305, CA, USA.
[7]Materials Science Division, Lawrence Berkeley National Laboratory, Berkeley, 94720, CA, USA.

*Corresponding author(s). E-mail(s): jhlee0667@lbl.gov; mary.scott@berkeley.edu; mwhittaker@lbl.gov;

Supplementary information

Supplementary Figures

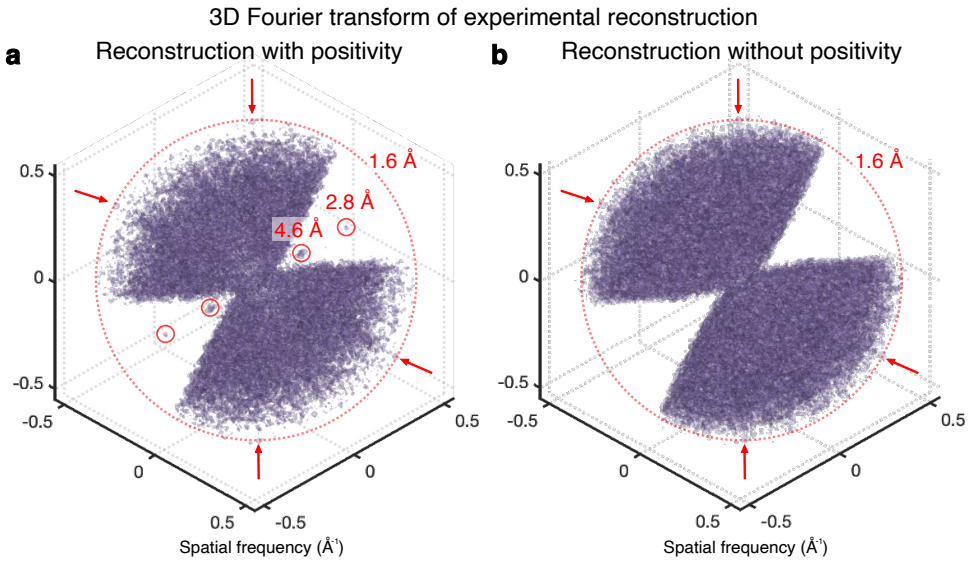

Fig. S1 Comparison of Missing Wedge Recovery with and without Positivity Constraint **a,** 3D Fourier transform of the experimental PhaseT∃M reconstruction of the Co_3O_4 nanoparticle shown in Fig. 2b, displaying recovered diffraction peaks within the missing wedge due to the positivity constraint. **b,** 3D Fourier transform of the reconstruction without the positivity constraint, showing no recovery of diffraction peaks in the missing wedge.

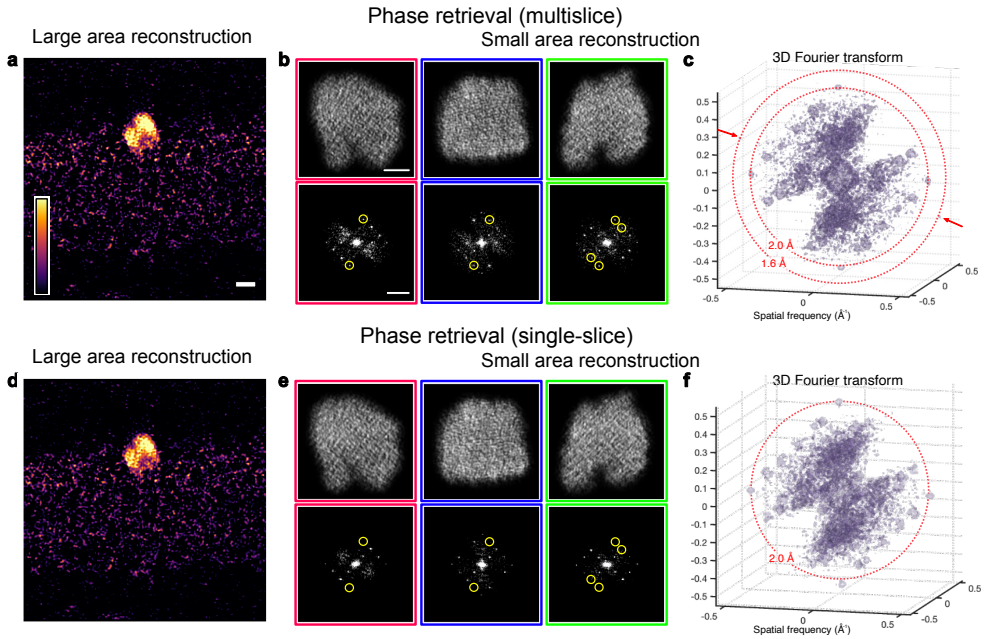

Fig. S2 Comparison of multislice and single-slice PhaseT∃M reconstructions. a, d, 4 Å-thick near-central 3D slices of the Co_3O_4 nanoparticle and its carbon support, reconstructed using the multislice (a) and single-slice (d) phase retrieval methods. Scale bar: 4 nm. **b, e,** 2 Å-thick slices extracted from the 3D reconstructions using multislice (b) and single-slice (e) phase retrieval methods. Slice colors correspond to the slice locations indicated in Fig. 2b–c. Yellow circles highlight diffraction peaks that are present only in the multislice reconstruction and absent in the single-slice result. Scale bar: 1 nm. **c, f,** 3D Fourier transforms of the reconstructions using the multislice (c) and single-slice (f) phase retrieval methods. Panel (c) is the same as shown in Fig. 2d. The 3D Fourier transform of the multislice reconstruction (c) shows a maximum resolution of 1.6 Å, whereas that of the single-slice reconstruction (f) shows a maximum resolution of 2.0 Å.

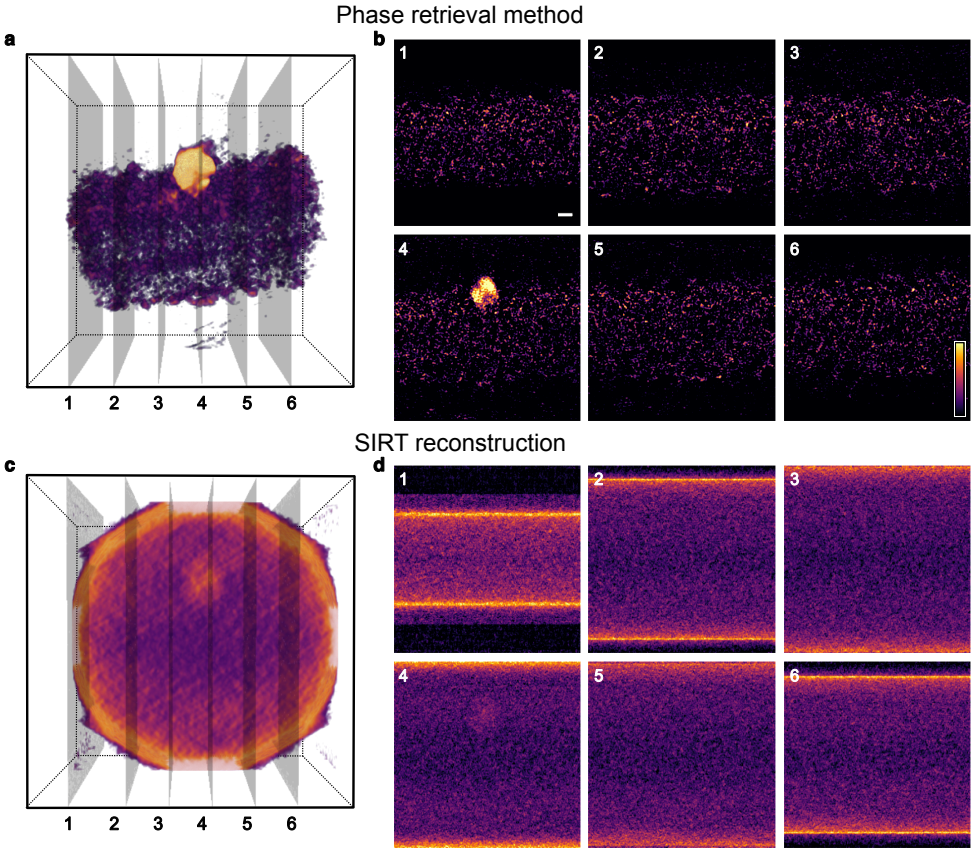

Fig. S3 Slices from Large-Area PhaseT∃M Reconstructions for the Co_3O_4 nanoparticle. **a, c,** 3D density maps of the Co_3O_4 nanoparticle and the carbon support reconstructed using phase retrieval (a) and SIRT (c). The 3D volumes were reconstructed with a voxel size of 2.08 Å. **b, d,** 4 Å-thick slices extracted from the 3D reconstructions in (a) and (c), respectively. The numbers in (a) and (c) indicate the slice positions corresponding to the numbered slices shown here. Scale bar: 4 nm.

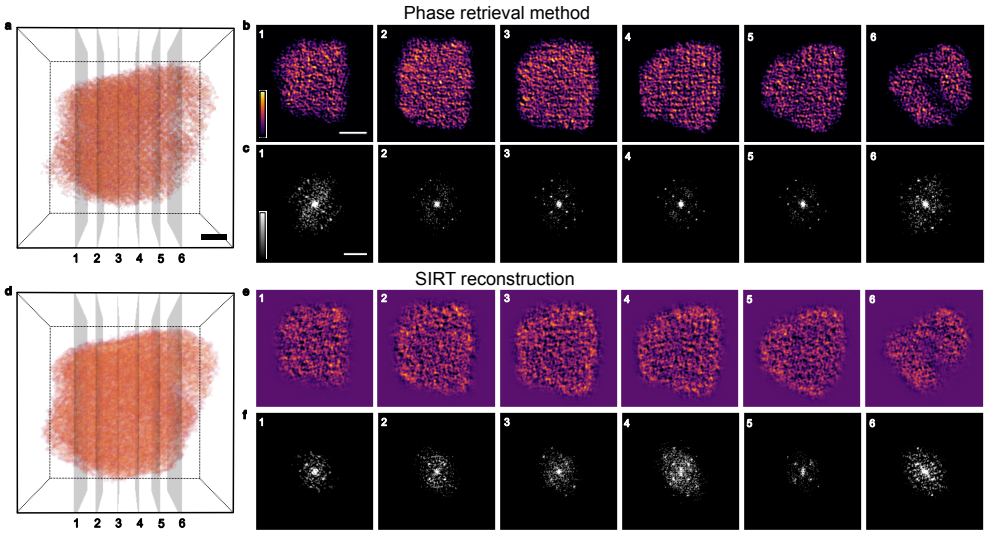

Fig. S4 Slices from Small-Area 3D PhaseT∃M Reconstructions of the Co_3O_4 nanoparticle and Their 2D Fourier Transforms. a, d, 3D density maps of the Co_3O_4 nanoparticle reconstructed using phase retrieval (a) and SIRT (f), after applying a 3D mask to remove the carbon support intensity. The volumes were reconstructed with a voxel size of 0.52 Å. Scale bar: 1 nm. **b, e,** 1 Å-thick slices extracted from the 3D reconstructions shown in (a) and (d), respectively. The slice numbers in (b) and (e) correspond to the positions indicated in the 3D reconstructions in (a) and (d), respectively. Scale bar: 2 nm **c, f,** 2D Fourier transforms of the slices in (b) and (e), respectively. Scale bar: 0.4 $Å^{-1}$.

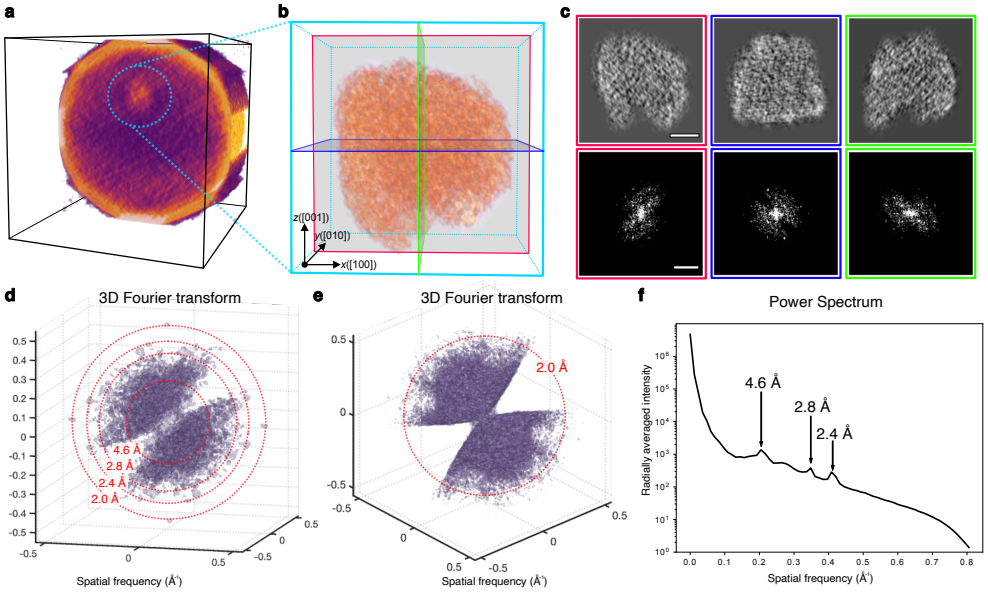

Fig. S5 Conventional SIRT Reconstruction and Resolution Analysis. a, Half-sectioned 3D density map illustrating the internal cross-section of the full 3D SIRT reconstruction of a Co_3O_4 nanoparticle embedded in a carbon support. **b,** 3D density map of the Co_3O_4 nanoparticle after applying a 3D mask to remove the carbon support. Scale bar: 1 nm. **c,** Top panel: 2-Å thick central slices of the 3D reconstruction in (b), with each color frame corresponding to the slice color in the 3D reconstruction. Bottom panel: 2D Fourier transform of the central slice shown in the top panel. Scale bars: Top panel, 2 nm; Bottom panel, 0.4 $Å^{-1}$. **d,** 3D Fourier transform of the reconstruction in (b), displaying diffraction peaks at 2.0 Å resolution. **e,** 3D Fourier transform of the reconstruction in (b) from a different view, highlighting the missing wedge region. The image clearly shows no diffraction peaks within the missing wedge. **f,** Power spectrum of the 3D reconstruction in (b), indicating a resolution of 2.4 Å.

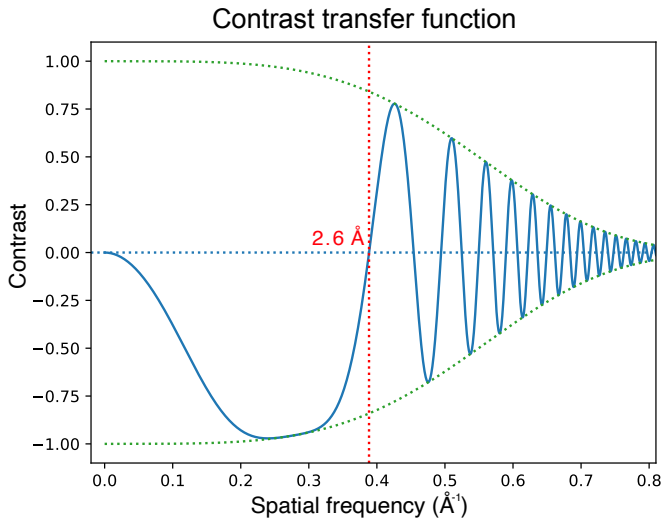

Fig. S6 Contrast transfer function (CTF) curve under the experimental conditions. The Scherzer defocus value was calculated using an optimized spherical aberration (C_3) value of 2.3 mm. The green dotted line represents the chromatic envelope function, computed using typical chromatic aberration (C_C) of 2.7 mm and an energy spread (ΔE) of 0.7 eV for the Titan Krios G3i microscope. The resulting contrast transfer function (CTF) indicates a diffraction-limited resolution of 2.6 Å.

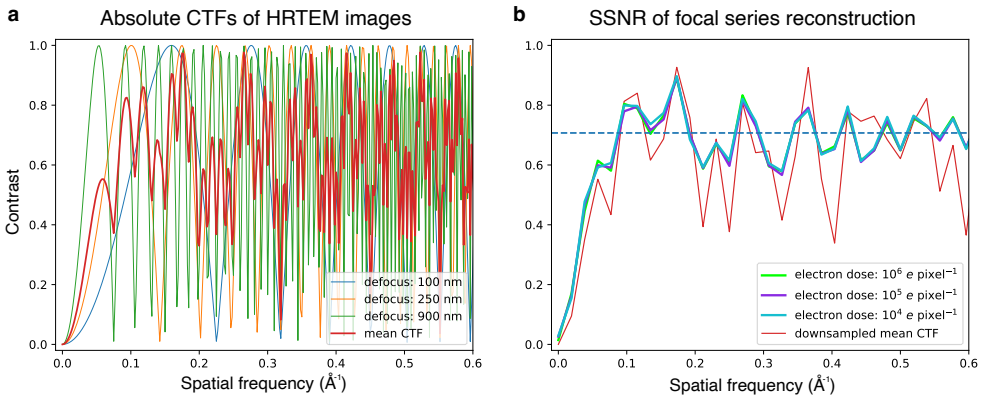

Fig. S7 Spectral Signal-to-Noise Ratio (SSNR) of 2D Focal Series Reconstruction. a, Simulated CTFs for defocus values of 100, 250, and 900 nm. **b,** SSNRs of focal series reconstructions using HRTEM images with defocus values of 100, 250, and 900 nm. For simplicity, the SSNRs of the focal series reconstruction are simulated under idealized conditions, assuming no chromatic aberration and using a single-slice reconstruction model.

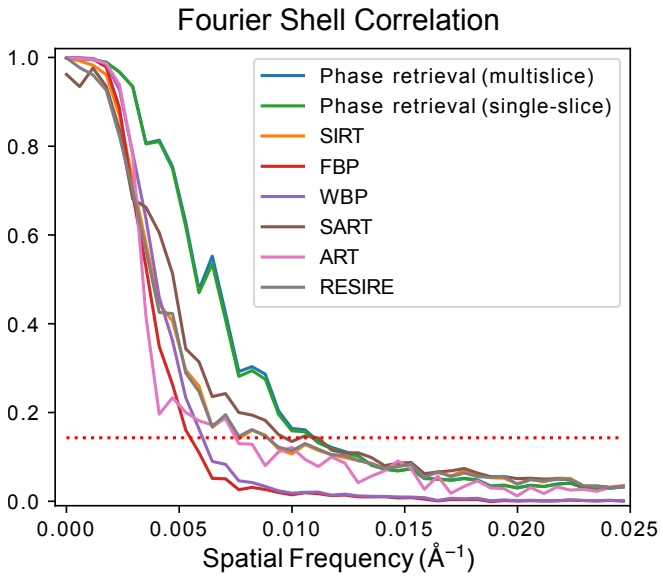

Fig. S8 Fourier shell correlation (FSC) from various reconstruction methods. FSC curves of HIV-1 particle reconstructions are compared across different methods: multislice phase retrieval (PhaseT∃M), single-slice phase retrieval (PhaseT∃M), simultaneous iterations reconstruction technique (SIRT), filtered back projection (FBP), weighted back projection (WBP), simultaneous algebraic reconstruction technique (SART), algebraic reconstruction technique (ART), and real space iterative reconstruction (RESIRE). The FSC resolutions, determined at the 0.143 criterion, are 9.0, 9.0, 13.1, 17.0, 15.5, 10.0, 13.1, and 10.6 nm, respectively.

Pseudo code for 3D reconstruction algorithm

Algorithm 1 Psuedo code to reconstruct 3D electrostatic potential

input : A tilt and focal series of measured HRTEM images $\{I_{\theta,\Delta f}\}$, Tilt angle set $\{\theta\}$, Defocus value set $\{\Delta f\}$,
Step size of the gradient descent method α,
Number of iterations: N_{iter}

output: 3D electrostatic potential $V(x,y,z)$

$V_{(1)}(x,y,z) \leftarrow 0$

`/* main reconstruction */`

$\psi_0(x,y) \leftarrow 1$ incident parallel electron wave function

$P(q_x,q_y) \leftarrow$ free-space propagation with thickness Δz (Eq. **??**)

for *i in {1 to* N_{iter}*}* **do**

  for θ *in tilt angle set* $\{\theta\}$ **do**

    $V_{\text{rot}}(x,y,z) = R_\theta V_{(i)}(x,y,z)$

    `/* forward propagation */`

    $\psi_1(x,y) \leftarrow \psi_0$ initial function

    $V_m^{\text{2D}}(x,y) \leftarrow$ projected potential set from $V_{\text{rot}}(x,y,z)$

    $\{t_m(x,y)\} \leftarrow$ transmission function set from $\{V_m^{\text{2D}}(x,y)\}$

    for *m in {1 to* N_z*}* **do**

      $\psi_{m+1}(x,y) \leftarrow \mathcal{F}^{-1}[P(q_x,q_y)\mathcal{F}[t_m(x,y)\,\psi_m(x,y)]]$

    end

    $\psi_{\text{exit},\theta}(x,y) \leftarrow \psi_{N_{z+1}}(x,y)$

    for Δf *in* $\{\Delta f\}$ **do**

      $\psi_{\text{final},\theta,\Delta f}(x,y) \leftarrow \mathcal{F}^{-1}[\psi_{\text{exit},\theta}(q_x,q_y)\exp(-i\chi(q_x,q_y))]$

      $\hat{I}_{\theta,\Delta f}(x,y) \leftarrow |\mathcal{F}(\psi_{\text{final},\theta,\Delta f}(x,y))|^2$

    end

    `/* backpropagation */`

    $\psi_{N_{z+1}}^{\text{back}}(q_x,q_y) \leftarrow \sum_{\Delta f}\exp(i\chi(\Delta f))\,\mathcal{F}\left(\psi_{\text{final},\theta,\Delta f} - \sqrt{I_{\theta,\Delta f}}\frac{\psi_{\text{final},\theta,\Delta f}}{|\psi_{\text{final},\theta,\Delta f}|}\right)$

    for *m in {*N_z *to 1}* **do**

      $\psi_m^{\text{back}}(x,y) \leftarrow \mathcal{F}^{-1}[P_m^*(q_x,q_y)\,\psi_{m+1}^{\text{back}}(q_x,q_y)]$

      $\nabla_V \mathcal{E}^2(x,y,m) \leftarrow \text{Re}\left(-i\,t_m^*(x,y)\,\psi_m^*(x,y)\,\psi_m^{\text{back}}(x,y)\right)$

      $\psi_m^{\text{back}}(q_x,q_y) \leftarrow \mathcal{F}[t_m^*(x,y)\;\psi_m^{\text{back}}(x,y)]$

    end

    `/* update 3D potential */`

    $V_{\text{rot}}(x,y,z) \leftarrow V_{\text{rot}}(x,y,z) - \alpha_V\,\nabla_V\mathcal{E}^2(x,y,z)$

    $V_{(i)}(x,y,z) \leftarrow R_\theta^{-1} V_{\text{rot}}(x,y,z)$

  end

end

$V(x,y,z) \leftarrow V_{(N_{\text{iter}})}(x,y,z)$